12 Surface Physics

T. Greber, J. Kröger, M. Hengsberger, J. Wider, H. J. Neff, C. Cepek, W. Auwärter, F. Baumberger, M. Hoesch, M. Muntwiler, I. Matsuda, R. Karrer, W. Deichmann, J. Osterwalder

Artificial nanostructures, exemplified e.g. by ultra-thin films, quantum wires or quantum dots, are of enormous scientific and technological interest. Their electronic and magnetic properties are dominated by size- and shape dependent quantum effects and can thus be tailored to fulfill any particular need. Their diameter in at least one dimension does not exceed a few atomic layers, and therefore they consist to a large extent of interfaces and surfaces.
In the surface physics laboratory we prepare clean surfaces, ultra-thin films and nanostructures under ultra-high vacuum (UHV) conditions and characterize their surface and interface structures at atomic resolution. Their electronic and magnetic properties are studied in detail. In order to measure the geometric arrangement of the atoms within the first few mono-layers of the surface we apply predominantly electron-based techniques such as x-ray photo-electron diffraction (XPD), medium-energy electron diffraction (MEED), low-energy electron diffraction (LEED), and more recently also scanning-tunneling and atomic force microscopy (STM/AFM). Angle-resolved UV photo-electron spectroscopy (ARUPS) gives us a detailed picture of the electronic band structure of such systems. Specifically, our experimental setup permits to directly map sections through the Fermi surface, which describes the electronic degrees of freedom relevant for transport properties, magnetic interactions and phase transitions. An important asset of such experiments is that the same probe (photoemission) gives structural, electronic and magnetic information, and we can therefore study the interplay between these different degrees of freedom on the same sample.

Over the past year we have continued our work on the following systems:

- Vicinal Cu(111) surfaces expose (111)-oriented terraces separated by a roughly regular array of mono-atomic steps, therefore they represent lateral nanostructures that can be easily prepared. We have studied the behaviour of the two-dimensional electron gas formed by a surface state in this well-defined and tunable potential energy landscape. In particular, the effect of the terrace size distribution on the measured surface state dispersion was studied (see Section 12.1).

- The quality and the electronic character of the interfaces are very important in metal-insulator heterojunctions, especially for magnetic devices based on junctions in which the tunneling barrier depends on the electron spin. A system, which has been thoroughly studied by our group is the Ni(111) surface covered with one mono-layer of hexagonal boron nitride (h-BN, see Sections 12.3, 12.4 and 12.5).

- In a collaboration with Prof. M. Sancrotti (TASC Laboratory of the Istituto Nazionale per la Fisica della Materia, Trieste, Italy) the structural properties of C_{60} mono-layer films on Ag(100) have been refined, and the coexistence of two inequivalent molecular orientations could be discovered by XPD [1].

Concurrent with these ongoing systematic studies, the development of several new experimental techniques has been pushed forward:

- Experimental near-node holograms could be measured in the new apparatus built in our laboratory (see Section 12.7). Nearest-neighbour atoms within a (111) plane of an Al crystal could be imaged at atomic resolution.

- Our picosecond time-resolved electron diffraction experiment is still in the phase where we struggle to enhance the surface sensitivity of the MEED technique. We have engaged in a strong collaboration with a group from Tohoku University (Japan). They have recently introduced a new three-dimensional MEED method that yields surface Patterson functions, thus revealing bonding vectors within the surface unit cells (see Section 12.8). In order to bypass these problems with surface sensitivity, a pulsed low-energy electron gun has been designed and tested which can be used for picosecond time-resolved LEED (see Section 12.9).

- We exploit our femtosecond Ti:sapphire laser system for introducing the same angle-mapping modes that we apply for ARUPS now also for two-photon photo-emission (2PPE) spectroscopy (see Section 12.4). These powerful measurement modes will give us unique capabilities for Fermi surface mapping at very low energies that can easily be extended to femtosecond time resolution.

- The construction and testing of our new experiment for spin-polarized Fermi surface mapping, which is designed to go eventually to the Surface and Interface Spectroscopy beamline of the Swiss Light Source, is progressing steadily. A sophisticated extraction electron optical system has been designed and is currently under construction (see Section 12.6). This experiment will permit the spin-resolved measurement of Fermi surfaces in magnetic nanostructures.

- We continued our collaboration with the surface chemistry group of Prof. J. R. Huber of the Physical Chemistry Department (P. Willmott, H. Spillmann) who have developed unique thin film preparation capabilities using pulsed reactive crossed-beam laser ablation. They have grown single crystalline films of zirconium carbonitrides (ZrC_xN_{1-x}) with the aim of correlating the hardness of these materials with their electronic structure as a function of the composition parameter x.

12.1 Fermi surfaces of the two–dimensional surface states on vicinal Cu(111)

The clean Cu(111) surface supports a free electron like Shockley–type surface state, with a maximum binding energy of ~ 0.4eV at $\bar{\Gamma}$. This state arises as a consequence of the broken translational symmetry in the normal direction at the crystal surface. Its wave functions propagate parallel to the surface with a Fermi wave length of $\lambda_F \sim 3$nm and fall off exponentially both towards the vacuum and towards the bulk and are thus quasi two-dimensional (2D).

We have continued our studies of the Shockley surface state on Cu(332) and Cu(221). Both surfaces are composed of (111) terraces bounded by mono-atomic steps running along $[1\bar{1}0]$. An analysis of the LEED spot profiles reveals a rather broad terrace width distribution, in agreement with an STM study [2]. The photo-emission Fermi surface map of Cu(332) in Fig. 12.1a shows a slightly elliptical, i.e. anisotropic surface state contour with a strongly angle dependent line-shape in the momentum distribution curves (Fig. 12.1b-c). The anisotropy of both, the dispersion and the line-width is less pronounced in the case of Cu(221).

We have developed a model for the surface state line-shape that includes the effects of the terrace width distribution [3]. Extensive 2D fits showed, that the anisotropic line-width can be fully attributed to the spatial averaging of the photo-emission experiment. However, an isotropic reduction of the photo-hole lifetime with decreasing terrace length and a remaining anisotropy in the dispersion on Cu(332) are intrinsic properties of the 2D electron gas in the 1D step lattice. The latter is strong evidence for the super-lattice sensitivity of the

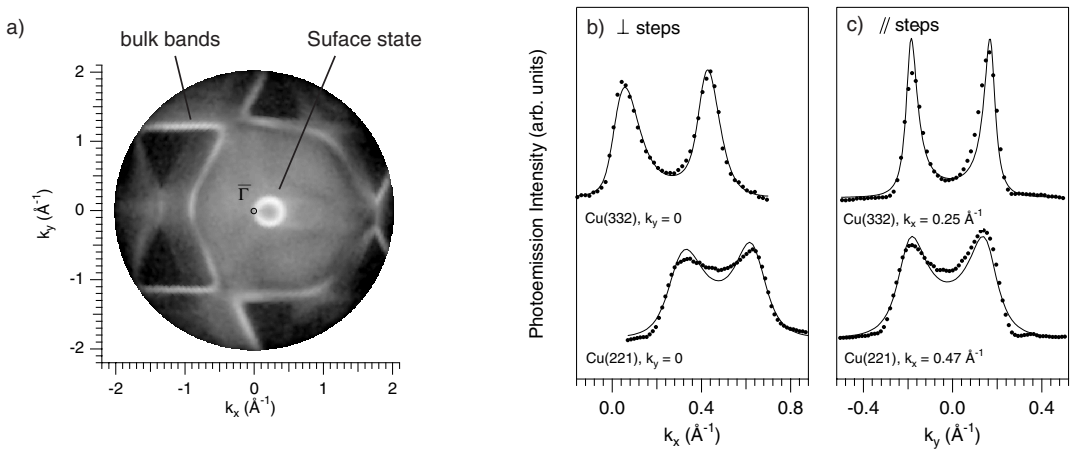

Figure 12.1: *a) Fermi surface map from Cu(332). b)–c) Momentum distribution curves at the Fermi level from Cu(332) and Cu(221). The data are all shown to scale. The thin lines are results from two–dimensional fits, including the effect of finite surface order.*

surface state. The reduced photo-hole lifetime on the other hand supports the scenario of a continuous surface state to surface resonance transition with increasing miscut away from the [111] direction, as it is expected from symmetry considerations.

12.2 Surface states and the stability of adsorbate periodicities: O/Mo(110)

In solid state physics, there is a lot of interest to understand materials properties and behaviour in relation to the shape and size of their Fermi surface. Quite interesting model systems can be found on metallic surfaces where complete Fermi surfaces can be mapped by photo-emission. A few years ago there was a study of an oxygen adsorbate phase on

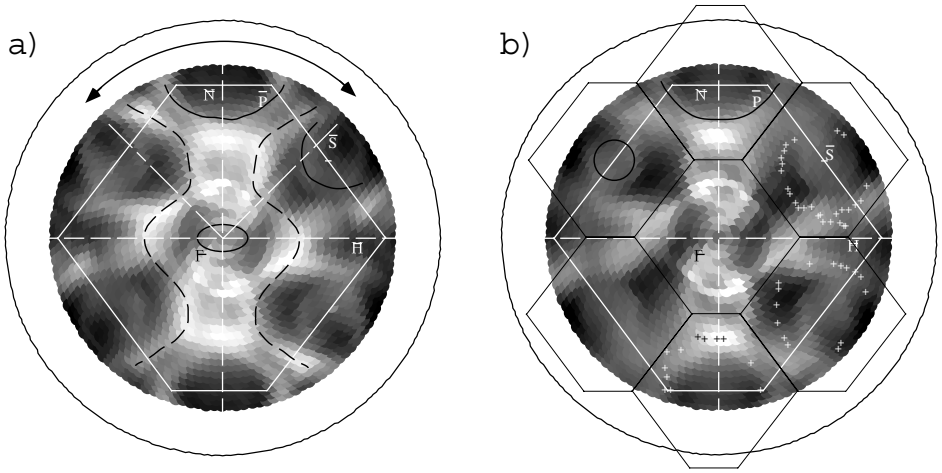

Figure 12.2: *a) He I excited Fermi surface map for clean Mo(110). The (1x1) surface Brillouin zone is indicated by white lines. The hole pockets and the electron pocket are marked as full and dashed black curves, respectively. b) Fermi surface map for p(2x2) O/Mo(110). Here, the boundaries of the (2x2) surface Brillouin zones are added as black lines. Some of the earlier photo-emission data [4] are included as small crosses.*

Mo(110), speculating that the high propensity of this system to form the (2x2) periodicity even at very low coverages is due to a *global Fermi surface nesting* [4]. This idea was supported by photo-emission data that indicated the presence of hole pockets centered at the $\bar{N}$ and $\bar{S}$ high symmetry points in the surface Brillouin zone that, though unrelated by the symmetry of the clean surface, create a perfect nesting scenario for a (2x2) superstructure due to their identical size and shape (see crosses in Fig. 12.2b).

This interpretation was recently challenged by new high-resolution electron energy loss measurements [5] that showed no indication for any softening of surface phonon modes around the $\bar{N}$ point or the $\bar{S}$ point for the p(2x2) phase that would be expected in this global nesting scenario. We have therefore redone the photo-emission experiment on this system, using our superior intensity mapping technique for tracking the Fermi surface contours [6]. In Fig. 12.2a, the measured contours from the clean Mo(110) surface are shown for reference. The Fermi surface map for the p(2x2) oxygen adsorbate phase in Fig. 12.2b gives no indication for the previously measured hole pockets (small white crosses) that have rendered this Fermi surface prone to nesting. In fact, there appear to be much more subtle changes to the surface states upon oxygen adsorption than for the case of hydrogen adsorption [7], where surface phonon softening was observed for two wave vectors that could clearly be related to nesting across Fermi surface sheets. The smaller influence of adsorbed oxygen on the surface states could be rationalized with the longer bond distance of the adsorbate to the Mo(110) top layer.

12.3 Tunneling across hexagonal boron nitride films on Ni(111)

in collaboration with G. Grad and P. Blaha, Institut für Physikalische und Theoretische Chemie, TU Wien

Hexagonal boron nitride (h-BN) is a wide band-gap insulator ($E_{gap} \approx 5\ eV$) that can be grown as single layers on Ni(111) [8, 9]. It serves as an ultimately thin model system for the investigation of spin polarized tunneling junctions. In Fig. 12.3a the known atomic structure

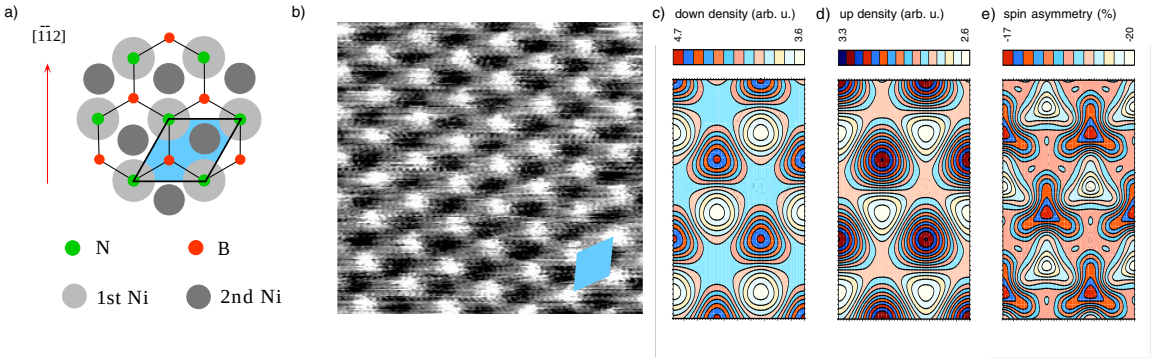

Figure 12.3: *h–BN on Ni(111): a) Top view of the honeycomb structure of h–BN on Ni(111). The (1x1) unit cell is indicated. b) Atomically resolved STM current image ($V_{tip} = 4.8meV$, $0.2 < I_t < 0.5nA$). The (1x1) unit cell is indicated. c) Calculated spin up density of states at E_F, 2.17 Å above the N layer. d) calculated spin down density of states at E_F, 2.17 Å above the N layer. e) Spin asymmetry of c) and d).*

is shown [9, 11, 10]. A single layer h-BN on Ni(111) is not thick enough to be insulating for electron transfer. This is seen from the fact that these surfaces can be imaged by scanning tunneling microscopy (STM) (see Fig. 12.3b) [9]. STM experiments showed atomically resolved images of h-BN/Ni(111). In the (1x1) unit cell ($a = 2.49\mathring{A}$) three distinct tunneling conductance levels were found. This translates into a charge density variation [12] that can be assigned to the images of three distinct sites: the nitrogen or top layer nickel site, the boron or *fcc* site, and the second layer nickel or *hcp* site. From our STM work it was not possible to identify the atomic species within the unit cell.

Density functional slab calculations for the h-BN/Ni(111) system solve this puzzle and give insight into the magnetism of this interface. In Fig. 12.3c the spin up (majority spin) density of states $\rho_\uparrow$ at $E_F \pm 60\ meV$, 2.17Å above the top N-layer is shown. The calculations identify the bright spots of highest conductance as the nitrogen sites and the grey spots to boron sites. The density functional calculations were spin polarized and therefore a spin asymmetry $A = (\rho_\uparrow - \rho_\downarrow)/(\rho_\uparrow + \rho_\downarrow)$ can be plotted (see Fig. 12.3e). The average asymmetry is -18.5 %, i.e. minority electrons prevail, and the variation at a distance of 2.17 Å above the top layer is 3 %.

12.4 Interface states in a metal-insulator heterojunction

In the h-BN monolayer on Ni(111) system, still little is known about the electronic states close to the Fermi level, especially in the unoccupied region. Two-photon-photoemission (2PPE) allows one to access both, occupied and unoccupied states, along with providing femtosecond temporal resolution from of a pulsed laser beam. Despite the advantages of the laser light source, the analysis of 2PPE spectra is less straightforward since three states are generally involved in one transition appearing as peak in the 2PPE spectrum.

In Fig. 12.4a, the normal emission 2PPE spectrum of h-BN/Ni(111) is shown in comparison to that of the bare Ni(111) surface. The spectrum from the h-BN covered sample extends over a larger energy range than that of clean Ni(111) due to the reduced work function. We want to focus our attention here onto the most prominent feature near the Fermi energy. The "counterpart" in the Ni spectrum appears at slightly higher binding energy, shifted by about 200 meV and with much less intensity. The peak in the Ni spectrum arises from a $\overline{\Gamma}$-surface state, which is spin split with occupation of only the majority spin states [13]. The huge intensity, however, of the peak in the h-BN spectrum gives evidence for the presence of an intermediate state in the 2PPE process since a slight tuning of the photon energy $h\nu$ causes a peak shift with $1 \times h\nu$ (see Fig. 12.4b). Preliminary analysis of the theoretical results shows this state to be an image potential state. This kind of state results from confinement of electrons between the crystal surface (band gap) and, on the vacuum side, the Coulomb potential of their own image charge in the crystal [14]. The energy of the hydrogen-like Rydberg series is tied, thereby, to the vacuum level as cut-off of the image potential and on the screening properties of the electrons in the crystal surface. From the 2PPE spectra one deduces a binding energy of roughly 600 meV as referred to the vacuum level. Full metallic screening as found e.g. on noble metal surfaces yields a maximum binding energy of 1/16 Ry = 850 meV for image potential states. The effective mass of this state, as estimated from dispersion plots along high-symmetry directions (Fig. 12.4c), is of the order of 0.5 times the free electron rest mass, thus smaller by a factor of 2 than the expected value for a free-electron-like image potential state. Further studies are necessary to determine the precise character of this state.

In order to verify the hypothesis of a strong intermediate state, 2PPE intensity maps have been recorded at fixed electron energy for various emission angles. One of these maps, taken at the 2P-Fermi energy, is displayed in Fig. 12.4d. The bright yellow ring should correspond

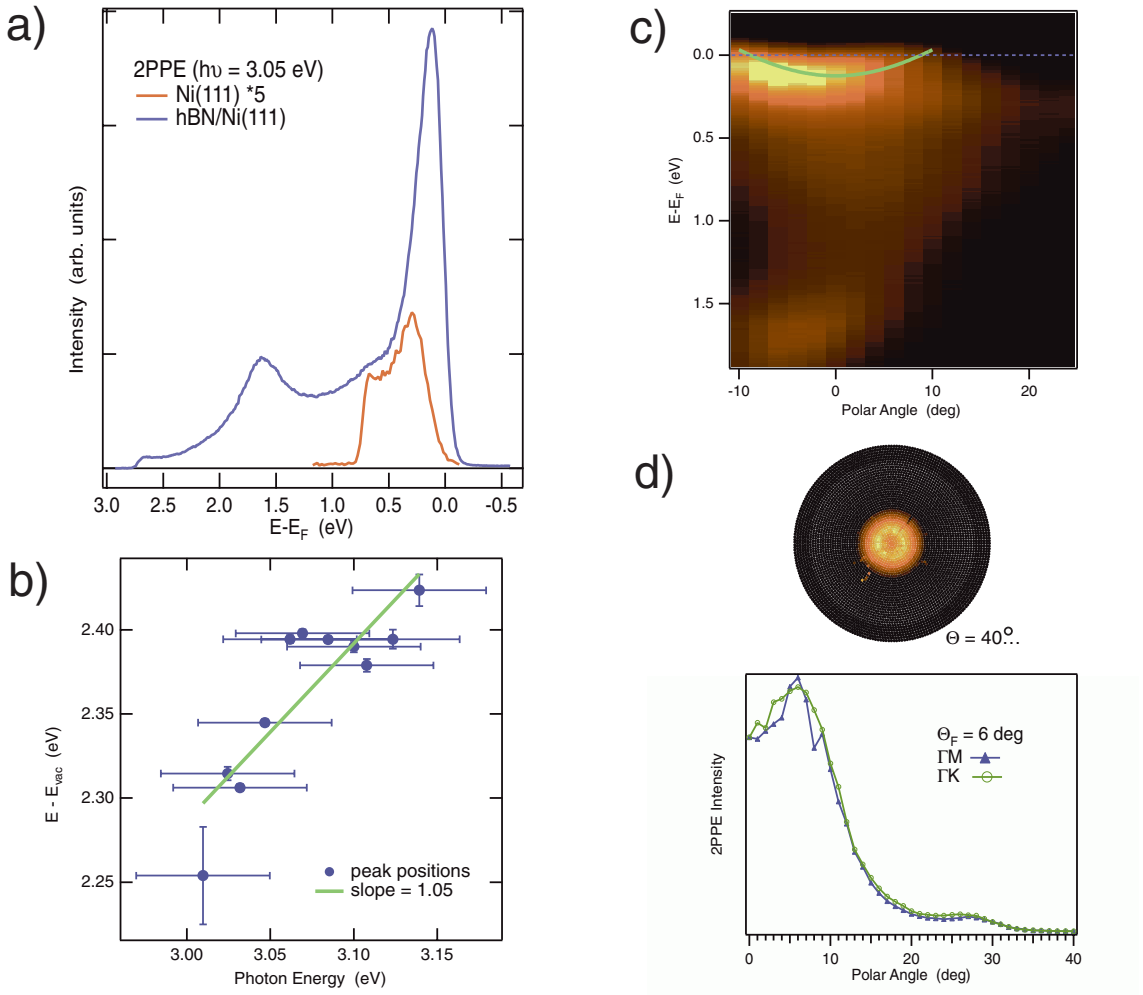

Figure 12.4: *Two-photon photoemission (2PPE) results from h-BN/Ni(111). a) Normal emission spectra ($h\nu = 3.1$ eV) from h-BN/Ni compared to that from Ni(111); b) shift of the prominent peak position with photon energy; c) angle-resolved spectra as colour plot (yellow = high intensity), taken along $\overline{\Gamma M}$ of the substrate together with the measured dispersion of the interface state (green line); d) two-dimensional map of the 2PPE intensity at the Fermi energy (upper panel) and two intensity profiles along high symmetry directions (lower panel).*

to a momentum of 0.127 Å^{-1}. In future experiments, this observed state can be used as a very sensitive probe of the dielectric properties of this interesting metal-insulator junction.

12.5 Co intercalation underneath hexagonal boron nitride films on Ni(111)

In order to study spin dependent tunneling, atomically well defined metal-insulator-metal structures have to be prepared. To produce a model system of a tunneling junction cobalt is evaporated on a mono-layer-thick hexagonal boron nitride (*h*-BN) film on a Ni(111) substrate [8, 9, 11]. STM measurements show that Co forms three-dimensional (3D) clusters at room temperature, while it prefers to grow in a more two-dimensional (2D) way at elevated temperature (150 °C). These two island types can coexist, as is seen in Fig. 12.5a. STM images give strong indications that intercalation of Co underneath the *h*-BN mono-layer is

responsible for the formation of different island types: defect lines, corrugated much less than the h-BN film thickness, are often found attached to the 2D islands (see Fig. 12.5a-b). These defects align to crystallographic directions and are related to the h-BN film: they can be seen on bare films but not on the clean Ni(111) substrate. From STM images showing sharp defect lines crossing 2D islands (as seen in Fig. 12.5b) it is concluded that these islands grow underneath the h-BN layer. This is consistent with missing forward scattering features in photo-electron diffraction patterns from the h-BN mono-layer with elevated-temperature deposits of Co.

Using the STM tip as a manipulator by working at small tunneling resistance, it is possible to remove the 3D Co clusters selectively one by one (see Fig. 12.5c). The 2D islands are not affected by this procedure and they are thus more strongly bound to the surface than the 3D clusters, again supporting the intercalation picture.

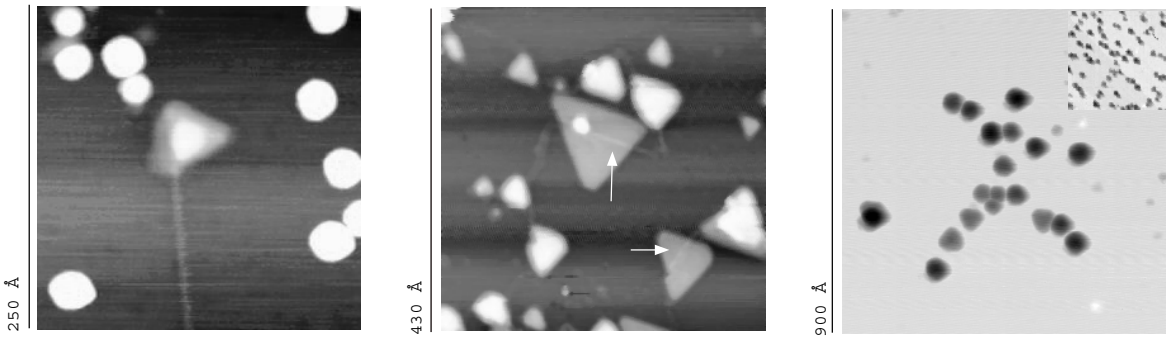

Figure 12.5: *STM images of Co on h-BN/Ni(111): Panel a) shows a two-dimensional triangular shaped island attached to a line defect coexisting with three dimensional Co clusters. In b) such defects are crossing two islands (marked by arrows). Panel c) (inverted gray scale) demonstrates the removal of three dimensional Co clusters by the STM tip (the inset represents the starting configuration)*

12.6 Status of COPHEE, the COmplete PHotoEmission Experiment

A new photo-electron spectrometer is being set-up featuring a full three-dimensional spin polarimeter, which makes it complete in the sense that all properties of the photoelectrons in the frame of reference of the sample crystal lattice can be measured. This apparatus is devoted to spin-resolved Fermi surface mapping using angle-resolved ultraviolet photo-electron spectroscopy. In this type of experiment, the sample and therefore also its magnetization direction are rotated over the full 2π solid angle above the crystal surface, thus requiring spin analysis in all three dimensions. After successful test operation using a He-lamp it is to be used as an end-station at the Surface and Interface Spectroscopy (SIS) beam-line of the new Swiss synchrotron radiation source (SLS) under construction at Paul Scherrer Institut, Villigen, or alternatively, at the Advanced Photo-emission Experiment (APE) beam-line at ELETTRA in Trieste.

UV-photoelectrons are energy and angle selected by a hemispherical analyzer (EA125 from Omicron Vakuumphysik GmbH) and then transported into a spin-polarimeter based on 60 keV Mott scattering (Mott detectors built by St. Petersburg Technical University [15]). The year 2000 was devoted to the design of the beam transport system, which leads the electrons from the EA125 exit slit to the two Mott detectors. In an electrostatic beam deflection system the spin-orientation in the laboratory frame remains constant and therefore two orthogonal polarimeters can determine the full three-dimensional spin-polarization

vector, since each Mott detector can intrinsically analyze the two components transverse to the respective incoming beam.

12.6.1 Electron optics

The electrons which travel at low pass energy (1 . . . 10 eV) inside the analyzer are accelerated to 300 times the pass energy in a two-step extraction lens behind the analyzer exit slit (lens made by Omicron). They are deflected by 90° to gain space for the bulky polarimeter. A gate lens provides vacuum safety for the gold foils inside the polarimeter and acts as an Einzel lens for the electron beam. The beam is deflected 20° to the left or right by a parallel plate deflector, which is switched at 20 . . . 0.1 Hz to allow quasi-simultaneous operation of the two detectors. An spherical end-deflector separates the two beams by ±45° for the required orthogonality. Inside the Mott detectors the electrons are accelerated to 60 keV by a spherical focusing field and detected by silicon diode detectors after back-scattering off an 80 nm gold foil. The lens elements and results of ray-tracing calculations are shown in Fig. 12.6.

The mechanical parts including the very demanding vacuum envelope are in production in the mechanical workshop. High voltage supplies such as the fast 2 kV polarity switch for quasi-simultaneous data acqusition have been manufactured by ISEG Spezialelektronik GmbH.

12.6.2 Data acquisition hard- and software

Besides controlling the various spectrometer devices (manipulator, energy analyzer, polarimeter optics, and detectors) photo-emission experiments at a synchrotron facility need to communicate with beam-line devices (storage ring, undulator, and monochromator). For this reason the SLS computing and control concepts are adopted in COPHEE. A VME system is the node for all electronic control and measurement signals of the spectrometer. It is operated by the Experimental Physics and Industrial Control System (EPICS) which provides a

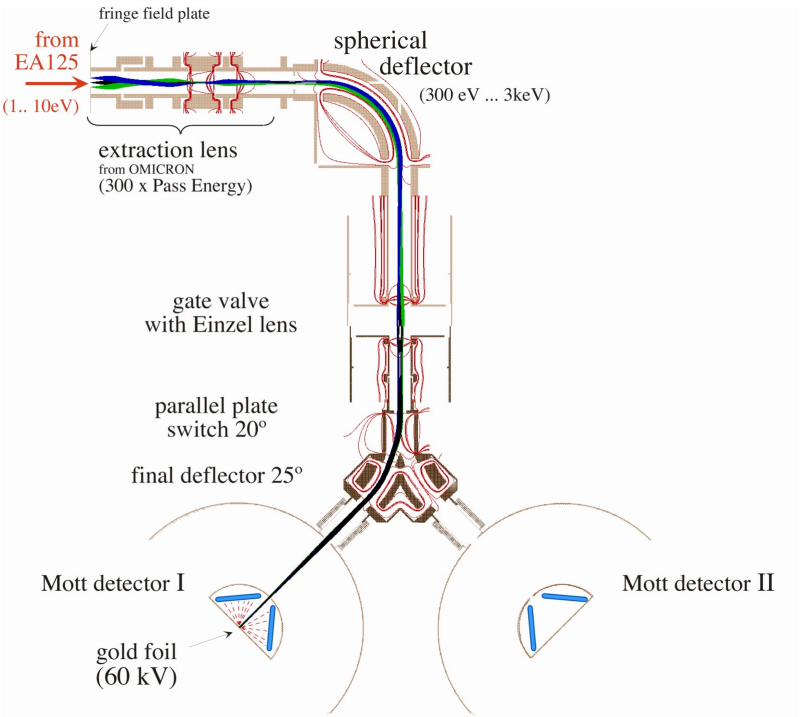

Figure 12.6: *Visualization of the ray-tracing calculations made to design the COPHEE electron optics (calculations and graphics by SIMION [16], 3D polarimeter assembly rotated 90° for graphical clarity)*

standardized and network-transparent interface to many different device types. Furthermore, fairly complex real-time tasks such as energy scans with synchronized detector readout are easily implemented on this level.

The high-level measurement control and the online data presentation for the sophisticated angle-scanned photo-emission experiments will be implemented in Delphi language on a remote personal computer. It is connected to the spectrometer simply via an Ethernet network using readily available interface software.

12.7 Near node photo-electron holography

Determining atomic structures at surfaces and interfaces is still a difficult but very important task. The more complex a system is, the more important it is to have direct methods that can provide a rough image of basic structural units. An angle scanned photo-electron diffraction experiment has all prerequisites for holography. The measured core-level photo-emission intensity is a coherent superposition of the directly emitted wave and the singly and multiply scattered waves. In the experimental realization of this idea several problems are encountered, caused by the strong and anisotropic nature of the electron-atom scattering amplitude and by multiple scattering effects. Near node photo-electron holography (NNPEH) [17] is a new approach to photo-electron holography that exploits the anisotropic nature of the electron source wave in order to minimize forward and multiple scattering effects. The idea has been successfully tested with an Al(111) single crystal in experiments at the synchrotron facility ELETTRA in Trieste, Italy [18]. Concurrently, a NNPEH experiment has been set up in our home lab. For unpolarized x-rays such as produced by a laboratory source, the near-node condition is met by having the electron escape direction very near the x-ray incidence direction, separated by only 10° to 20°. First results, again with an Al(111) single crystal, are presented in Fig. 12.7. In the holographic reconstruction (Fig. 12.7b) the six nearest neighbors of an Al atom within the (111) crystal plane are clearly resolved.

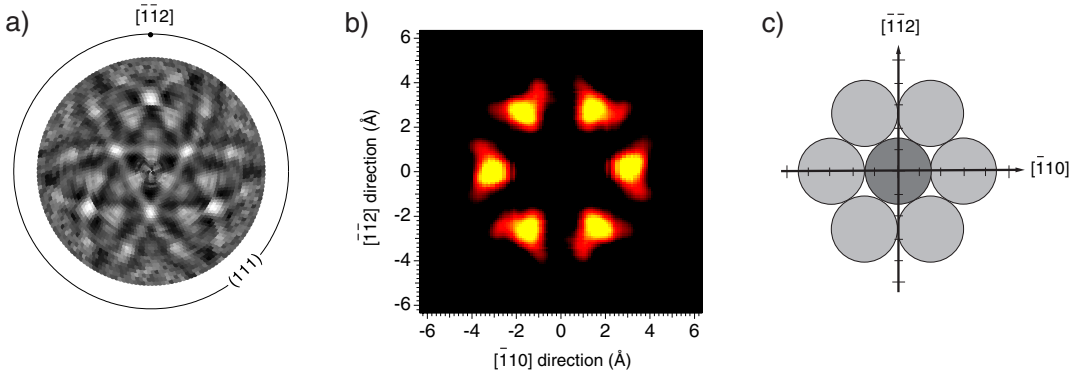

Figure 12.7: *a) Stereographically projected experimental Al 2s (E_{kin} = 1370 eV) photo-electron diffraction pattern from an Al (111) single crystal. b) Corresponding holographic real space reconstruction of a plane parallel to the surface containing the emitter at the origin (0, 0). The six nearest neighbors are clearly resolved at a distance of 3.2 Å. Note that the photo-emitter is not imaged in photo-electron holography. c) Hard sphere model of a (111) plane of an aluminum crystal.*

12.8 Surface Patterson functions from medium-energy electron diffraction

in collaboration with T. Abukawa, S. Kono, Tohoku University, Sendai, Japan

We have continued our project to develop a picosecond time-resolved electron diffraction experiment for studying surface dynamics. In the process we were facing the problem that the standard medium-energy electron diffraction (MEED) experiment did not yield the required mono-layer structural sensitivity. Recently, a Japanese group introduced an new structural tool based on multiple-energy, full three-dimensional diffraction images that can be Fourier transformed to yield Patterson functions very similar to those obtained from x-ray diffraction [19]. In a close collaboration with this group we have adopted this method, using our pulsed MEED electron gun. In a first test experiment we have successfully measured nearest neighbor bond vectors within a Ge(111) surface. In Fig. 12.8a a section through a three-dimensional data set of scattering intensities is shown. The experimental geometry, i.e. the incoming electron beam direction and the position of the two-dimensional detector determines which atoms can be imaged. The data set of Fig. 12.8a is sensitive to the geometry normal to the crystal surface. The planar section through the Patterson function in Fig. 12.8c displays clearly the nearest neighbour bond direction and bond length along the (111) direction. The extension of such experiments to picosecond time resolution is straightforward using a pump-probe approach.

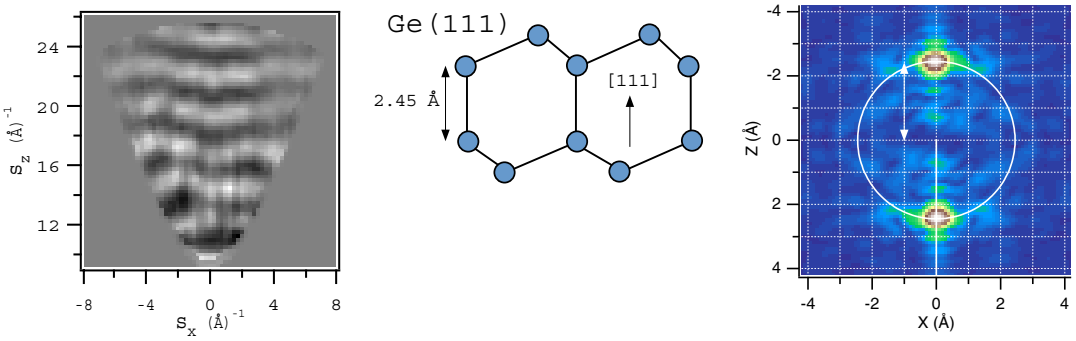

Figure 12.8: *a) Normalized scattering intensities of electrons backscattered from a Ge(111) surface, plotted as a function of the scattering vector* $\vec{s} = \vec{k}_f - \vec{k}_i$ *where* $\vec{k}_f$ *and* $\vec{k}_i$ *are scattered and incoming electron wave vectors, respectively. b) Planar view of the Ge crystal structure, indicating the 2.45 Å between nearest neighbor atoms along the (111) direction. Patterson function obtained from Fourier transforming a full three-dimensional set of scattering intensities. The white arrow indicates the bond distance along the (111) direction.*

12.9 Construction of an electron gun for time resolved low-energy electron diffraction

A second option for enhancing the surface sensitivity of electron diffraction is to go to lower energies. The standard tool for structure determination in surface physics is low energy electron diffraction (LEED), where energies of typically 50 eV - 150 eV are used. However, it is a very demanding task to prepare picosecond pulses of electrons at such low energies. An miniaturized electron gun which produces ultra short and coherent (parallel and monochromatic) electron pulses with an expected time resolution of less than 5 ps has been developed in our lab.

Through the back side of the electron gun, femtosecond laser pulses (80 fs, 400 nm wave length) are directed through a sapphire window onto a photo-cathode, which consists of a atomically flat and thin ($\sim$ 200 Å) gold film grown on a mica substrate. The laser beam is transmitted from behind through the mica plate and photoelectrons are emitted from the gold-vacuum interface by two-photon photo-emission. These electrons are accelerated to a kinetic energy of 100 eV over a distance of less than 100 μm from where they move in field free space towards the sample. The calculated temporal jitter within the electron pulses is less than 3 ps for a sample placed at a distance of 4 mm from the photo-cathode. The main contribution is due to the energy spread of the electrons, which has been optimized by choosing gold as cathode material. The vacuum part of the gun is shown in Fig. 12.9. The actual electron gun is in the tip of the metal cone, while the whole setup is much bigger for functionality.

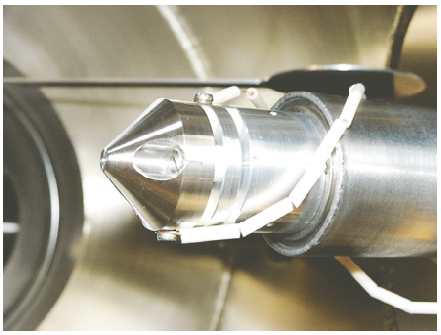

Figure 12.9: *The vacuum end of the picosecond low-energy electron gun.*

The gun has been designed, built and tested [20]. For this purpose, the electron beam has been directed onto a two-dimensional position-sensitive channel-plate detector, placed 65 mm away from the gun. From the spot size of the beam on the detector (Fig. 12.10) the divergence is calculated to be about 1.5°. In these tests, the following specifications could be

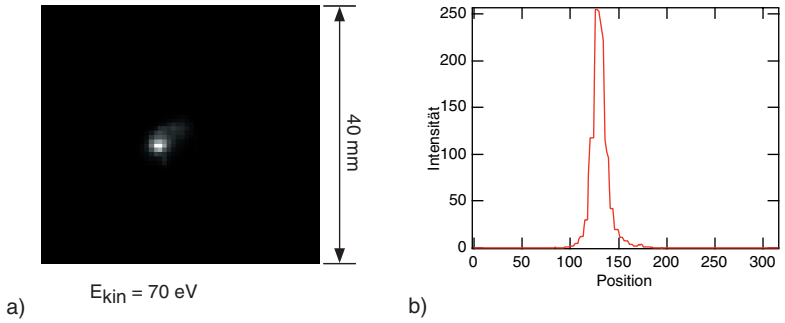

Figure 12.10: *a) The electron beam profile for an energy of 70 eV, measured with a two-dimensional detector placed at a distance of 65 mm from the electron gun. b) Beam cross section, from which the beam divergence of* 1.5° *was determined.*

demonstrated [20]: A very low electron current of about 2 fA was measured on the detector. The measured energy resolution is about 1.3 eV, a part of which is likely to be due to the resolution of the detector. With this energy spread, the time resolution should be less than 4 ps. The gun therefore meets the design criteria and, if the electron current can be increased by one or two orders of magnitude, the picosecond LEED experiment is within reach.

References

[1] C. Cepek, R. Fasel, M. Sancrotti, T. Greber, J. Osterwalder, Phys. Rev. B 63, 125406 (2001).

[2] A.R. Bachmann, A. Mugarza, J.E. Ortega, A. Närmann, S. Speller, Phys. Rev. B, submitted

[3] F. Baumberger, T. Greber, and J. Osterwalder, Phys. Rev. B, submitted

[4] S. Dhar, K.E. Smith, S.D. Kevan, Phys. Rev. Lett. 73, 1448 (1994).

[5] J. Kröger, S. Lehwald, H. Ibach, Phys. Rev. B 58, 1578 (1998).

[6] J. Kröger, T. Greber, J. Osterwalder, Surf. Sci. 459, 173 (2000).

[7] J. Kröger, T. Greber, J. Osterwalder, Phys. Rev. B 61, 14146 (2000).

[8] A. Nagashima, N. Tejima, Y. Gamou, T. Kawai, and C. Oshima, Phys. Rev. B 51, 4606 (1995).

[9] W. Auwärter, T.J. Kreutz, T. Greber, J. Osterwalder , Surf. Sci. 429, 229 (1999).

[10] Y. Gamou, M. Terai, A. Nagashima, and C. Oshima, Sci. Rep. RITU, A 44, 211 (1997).

[11] M. Muntwiler, W. Auwärter, F. Baumberger, M. Hoesch, T. Greber and J. Osterwalder, Surf. Sci. 472, 125 (2000).

[12] J. Tersoff, D.R. Hamann, Phys. Rev. B 31, 805 (1985).

[13] M. Donath, Surf. Sci. Rep. 20, 251 (1994).

[14] T. Fauster, in *Electronic Surface and Interface States on Metallic Systems*, edited by E. Bertel and M. Donath (World Scientific, Singapore 1995), p. 171.

[15] V.N. Petrov, M. Landolt, M.S. Galaktionov, B.V. Yushenkov, Rev. Sci. Instr. 68, 4385 (1997).

[16] "SIMION 3D Version 6.0" by David A. Dahl 43ed ASMS Conference on Mass Spectrometry and Allied Topics, May 21-26 1995, Atlanta, Georgia, pg 717, http://www.srv.net/ klack/simion.html

[17] T. Greber, J. Osterwalder, Chem. Phys. Lett. 256, 653 (1996).

[18] J. Wider, F. Baumberger, M. Sambi, R. Gotter, A. Verdini, F. Bruno, D. Cvetko, A. Morgante, T. Greber, J. Osterwalder, Phys. Rev. Lett. 86, 2337 (2001).

[19] T. Abukawa, C.M. Wei, T. Hanano, S. Kono, Phys. Rev. Lett. 82, 335 (1999).

[20] R. Karrer, *Bau einer Elektronenkanone für zeitaufgelöste Beugung mit langsamen Elektronen (LEED)*, Diplomarbeit Uni Zürich, 2000.